Time-independent and time-dependent photoassociation of spin-polarized rubidium



1999 J. Phys. B: At. Mol. Opt. Phys. 32 287

(http://iopscience.iop.org/0953-4075/32/2/012)

J. Phys. B: At. Mol. Opt. Phys. **32** (1999) 287–308. Printed in the UK PII: S0953-4075(99)93290-X

# Time-independent and time-dependent photoassociation of spin-polarized rubidium

H M J M Boesten†, C C Tsai‡, D J Heinzen‡, A J Moonen† and B J Verhaar†

† Eindhoven University of Technology, Box 513, 5600 MB Eindhoven, The Netherlands
‡ Department of Physics, The University of Texas, Austin, TX 78712, USA

Received 15 April 1998, in final form 15 September 1998

**Abstract.** We extract information about collisions of ultra-cold ground-state rubidium atoms from observations of a g-wave shape resonance in the $^{85}$Rb + $^{85}$Rb system via time-independent and time-dependent photoassociation. The shape resonance arises from a quasi-bound state inside a centrifugal barrier that enhances the excitation to the bound electronically excited state by the photoassociation laser in the time-independent experiment. The shape resonance is sufficiently long-lived that its build-up through the barrier can be observed by first depleting it via a photoassociation laser pulse and then measuring the rate of photoassociation by a second laser pulse with a variable delay time. A combined method of analysis of the time-independent and time-dependent experiments is presented. We discuss the spectroscopy of states of two particles with spin trapped inside a centrifugal barrier, interacting via direct and indirect spin–spin interactions.

## 1. Introduction

Interactions between ground-state alkali atoms play a key role in many experiments in cold-atom physics. The accuracy of atomic clocks based on an atomic fountain of laser-cooled Cs atoms, for instance, is limited by frequency shifts due to binary collisions between the atoms during their fountain orbit [1]. Atomic interaction processes are also crucial for Bose–Einstein condensation in magnetic traps [2–4]: they determine the stability or instability of the Bose condensate via the sign and magnitude of the condensate self-interaction, and also the inelastic rates for transitions from trapped to untrapped states. A number of methods are available to obtain information on such interaction processes. A very powerful method is based on the cold-atom photoassociation process [5–11]. In this free–bound transition process two colliding ground-state atoms are excited by a photoassociation (PA) laser to a bound electronically excited state. Due to the Franck–Condon principle, the excitation occurs preferably near the outer turning point $r_0$ of the excited state, where the atoms have a velocity comparable to that in the ground-state channel. A direct consequence is that the excitation probability is approximately proportional to the ground-state collisional radial wavefunction squared at this outer turning point, which enables one to map out the nodal structure of this wavefunction along a frequency axis. This approximation can be improved by calculating a radial transition integral, which is common practice in analysing cold-atom PA experiments [11]. Figure 1 shows a presentation of radial wavefunctions of the ground state and the excited state, together with their above-mentioned Franck–Condon relationship.

0953-4075/99/020287+22$19.50  

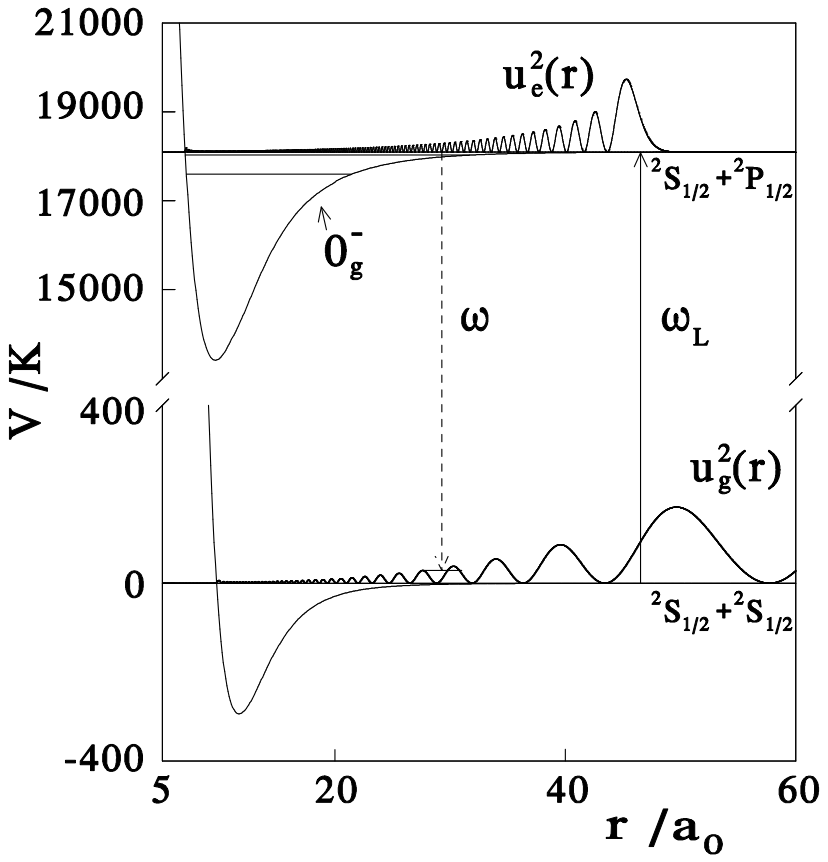


**Figure 1.** Cold-atom photoassociation. Excitation of a colliding pair of Rb atoms by a photon ($\omega_L$) leads to the formation of an excited $Rb_2$ molecule in the $0_g^-$ excited-state potential and is followed by spontaneous decay (frequency $\omega$). The square of the ground-state radial wavefunction $u_g^2(r)$ of the initial collisional state and of the excited-state radial wavefunction $u_e^2(r)$ are shown.

The actual application of this simple idea still leads to a very complicated situation because of several facts:

(a) The hyperfine structure of the excited electronic states, the so-called hyperfine 'spaghetti' [12].
(b) the difficulty of determining a large number of combined triplet and singlet parameters in the ground-state collision simultaneously;
(c) the fact that several ground-state partial waves $l$, ranging from $J-2$ (or 0) to $J+2$, contribute to the excitation of a single rovibrational excited-state $v, J$. This is due to two circumstances:

- the electronic spins contribute to the total molecular angular momentum;
- the laser photon inducing the transition introduces an angular momentum $1\hbar$ into the system with, in principle, various orientations relative to the initial angular momentum of the two-atom system.

As a consequence, by angular momentum conservation, each $J$ peak can be reached starting from non-negative $l$ values ranging from $J-2$ to $J+2$.

By a careful choice of experimental circumstances we have been able to eliminate all three complications [10]. The first step is to doubly polarize the ground-state atoms, i.e. to prepare them in the hyperfine state with fully stretched electronic and nuclear spins along a magnetic field $\vec{B}$ with optical pumping lasers. In this way only the triplet spin state in the initial channel is involved, thus avoiding complication (b).

The second step is to concentrate on the excitation of a suitable excited electronic state: the $0_g^-$ state connected with the $^2S_{1/2} + {}^2P_{1/2}$ separated-atom limit (we will refer to this state as the lower $0_g^-$ state). The structure of this and all other excited states associated with the $^2S + {}^2P$ separated-atom limits has been studied by Movre and Pichler [13]. In the radial range of outer turning points of the highest $0_g^-(^2S_{1/2} + {}^2P_{1/2})$ rovibrational states observed, ranging from 41 $a_0$ to 48 $a_0$, this electronic state has a very simple structure, determined by a $2 \times 2$ eigenvalue problem containing the fine-structure splitting of the excited atom and the interatomic $1/r^3$ resonant electric dipole interaction. Due to the fact that the fine-structure splitting dominates, the structure of the electronic state considered is simply given by the product of the separated-atom states

$$\left[\left(^2S_{1/2}\{1A\}\,{}^2P_{1/2}\{2B\}\right)_{j=0} - \left(^2S_{1/2}\{1B\}\,{}^2P_{1/2}\{2A\}\right)_{j=0}\right]/\sqrt{2} \tag{1}$$

antisymmetrized in 1 and 2, with the electronic angular momenta $\frac{1}{2}$ coupled to total $j = 0$. The notation 1A, for instance, signifies that the set of electrons 1 occupies the indicated state around nucleus A. The angular-momentum coupling and the subtraction in the above expression together assure the correct symmetry properties corresponding to the quantum numbers $0_g^-$. As pointed out in [14], to our knowledge this is the first observed example of a Hund's (e) case in the literature, i.e. both the total electronic angular momentum $j$ and the rotational angular momentum have definite values. The latter is conserved in the PA excitation process, so that $J$ equals the ground-state $l$ value, thus avoiding complication (c): each photoassociation peak $J$ is the direct probe of the ground-state radial wavefunction for a single $l$.

Another advantage of the above choice of excited state is that it is a pure triplet state [13]. We conclude that the laser does not introduce a singlet admixture, which would spoil the above pure triplet situation in higher order in the laser intensity, a complication that would occur in the analysis of the time-dependent experiment in the following.

By the same choice of excited state, complication (a) is avoided. The vanishing $\Omega$ and $j$ values imply that in very good approximation the nuclear spins are decoupled from the remaining angular momenta. The hyperfine splitting is only second order and no complex hyperfine-coupled problem needs to be handled in the final state. By the unique initial nuclear spin state only the fully nuclear-spin polarized final state contributes.

Due to the vanishing $j$ value, the total electronic angular momentum before the excitation, i.e. the vector sum of the electronic spins, is equal to minus the angular momentum of the dipole PA photon absorbed. Using a PA laser beam propagating in the direction of the static magnetic field $\vec{B}$ and preparing the ground-state atoms in the hyperfine state with fully stretched electronic and nuclear spins along $\vec{B}$, we therefore find that a right-circularly polarized PA beam does not lead to excitation, in contrast to a left-circularly or linearly polarized one. This was observed experimentally [10]. Experimentally, we also find that only even $J$ rotationally resolved states are excited, in agreement with Bose symmetry in the (spin-symmetric) ground-state channel. We thus achieve our goal: we are able to study the nodal structure in a single ground-state channel by mapping it out as a function of the laser frequency.

In [10] we have been able, using the above approach, to make the first predictions for the triplet scattering length $a_T$ for binary collisions of $^{85}$Rb atoms and, making use of a mass-scaling rule, also for $^{87}$Rb atoms. The PA excitation probability is measured by having the PA laser beam on intermittently with a far off resonance trapping (FORT) laser and two optical

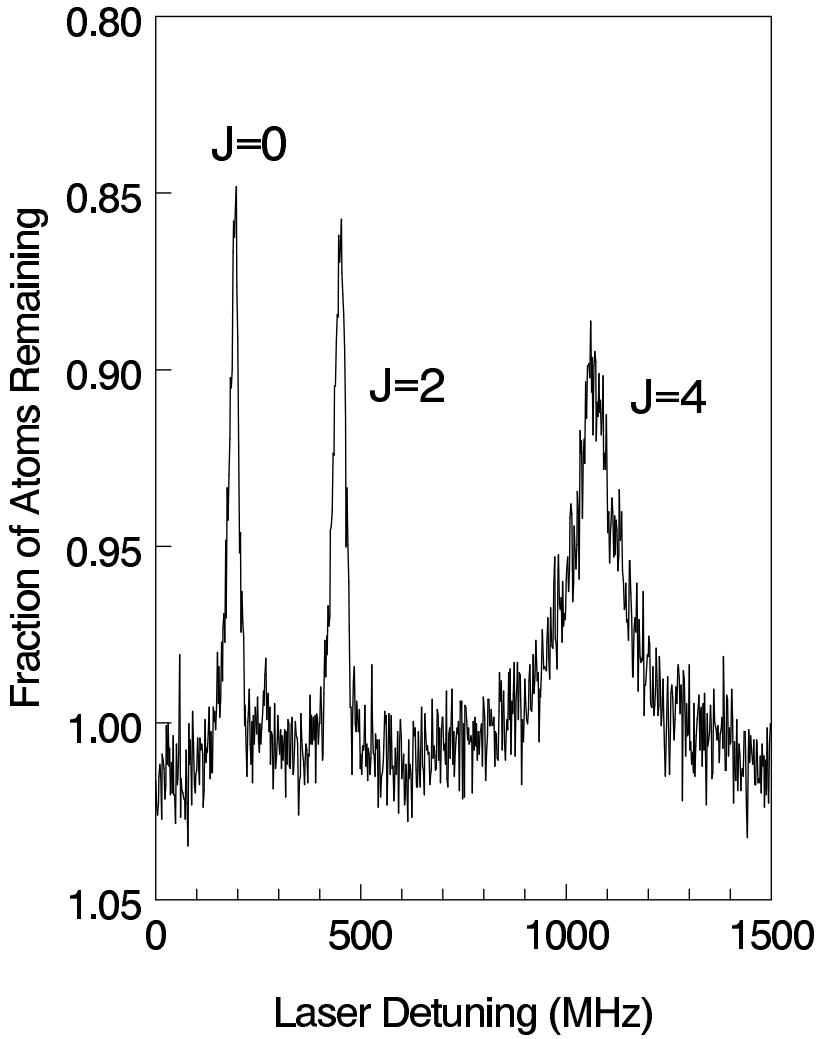


**Figure 2.** Photoassociation spectrum of the $0_g^-$ vibrational level at $-5.812$ cm$^{-1}$, relative to the barycentre of the $S_{1/2}$ + $P_{1/2}$ dissociation limit, for the collision of spin-polarized $^{85}$Rb atoms. Notice the absence of odd rotational lines due to Bose statistics.

pumping laser beams during a certain time period. The number of atoms remaining in the trap is reduced, because virtually all excited pairs of atoms decay spontaneously to free pairs with a kinetic energy that is too large to remain in the trap (frequency $\omega$ in figure 1). Probing the atoms with laser-induced fluorescence, this results in a detectable change in the fluorescence level, i.e. in a measurement of the photoassociation loss rate. Figure 2 shows an experimental rotationally resolved PA spectrum for a vibrational state of the lower $0_g^-$ state, measured using a linearly polarized PA laser beam. In contrast to the case without optical pumping only even $J$ peaks occur.

The unique relation between $J$ and $l$ thus realized makes it possible to simplify the analysis considerably. In a dressed-state picture, represented schematically in figure 3, either the bound excited level is shifted downward by the laser photon energy $\hbar\omega_L$ or the ground-state potential

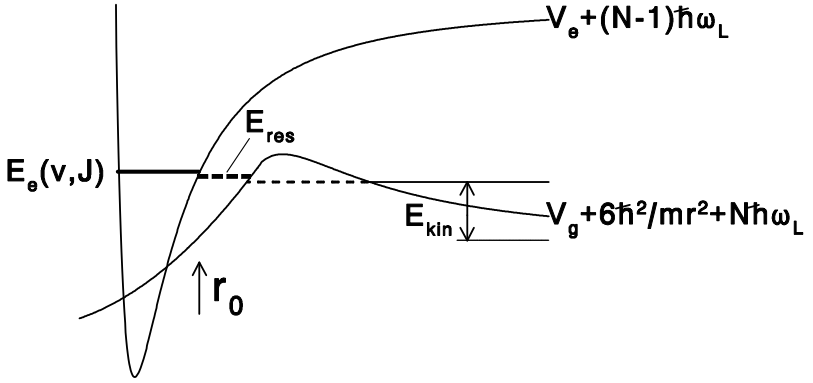


**Figure 3.** Dressed-states picture of the photoassociation process, including schematic ground-state ($V_g + 6\hbar^2/mr^2$ for $l = 2$) and excited-state ($V_e$) potentials. Changing the laser frequency $\omega_L$, the excited bound state energy $E_e(v, J)$ with vibrational quantum number $v$, rotational quantum number $J$ and outer turning point $r_0$, shifts over the Maxwellian energy distribution in the incoming channel. The bold broken line indicates the position of the shape resonance $E_{res}$.

is shifted upward by the same energy (the resonance level $E_{res}$ within the centrifugal barrier will be discussed in the following section). It thus becomes clear that the bound excited state, which already has a finite width $\gamma_0$ for spontaneous emission, is embedded in the ground-state continuum and thus turns into a Feshbach resonance [15] with an additional width $\gamma_L$ for laser-induced continuum decay.

While the observed $^{85}$Rb PA spectrum contained $J = 0, 2, 4$ rotational peaks, we used only the $J = 0, 2$ peaks in the previous analysis of [10]. The $J = 4$ peak in the $^{85}$Rb PA spectrum showed anomalous features, i.e. a larger width and a much lower saturation intensity, which precluded an analysis along the same lines. In [14, 16] we recognized the anomaly, as well as a similar anomalous $J = 2$ peak in the $^{87}$Rb PA spectrum, as being due to a shape resonance in the ground-state channel. In this paper we will focus on the special possibilities that arise for obtaining important information on interactions of cold Rb atoms from the exceptionally long lifetime of the shape resonance in the $^{85}$Rb + $^{85}$Rb system. On the experimental side this adds the possibility of a pulsed photoassociation experiment to the usual type of time-independent photoassociation experiment, yielding completely new information. On the theoretical side inelastic processes with a time scale too slow to play a significant role during an elastic collision in the usual type of photoassociation experiment, start to contribute significantly, opening the possibility to study a larger set of cold-collision properties. A brief description of the present work was presented in [14].

This paper is organized as follows. In section 2 we discuss the concept of shape resonance. Section 3 is devoted to a determination of excited-state parameters needed for further analysis. In section 4 we discuss the decay mechanisms of the $^{85}$Rb g-wave shape resonance and include them in the analysis of the time-independent and the time-dependent photoassociation experiments. Conclusions are presented in section 5.

## 2. Shape resonances

When two atoms collide via a partial-wave $l \neq 0$ a long-lived state inside the centrifugal barrier may form during the collision process. Such a state is commonly referred to as a shape resonance. Figure 3 shows, in addition, a schematic picture of a shape resonance in

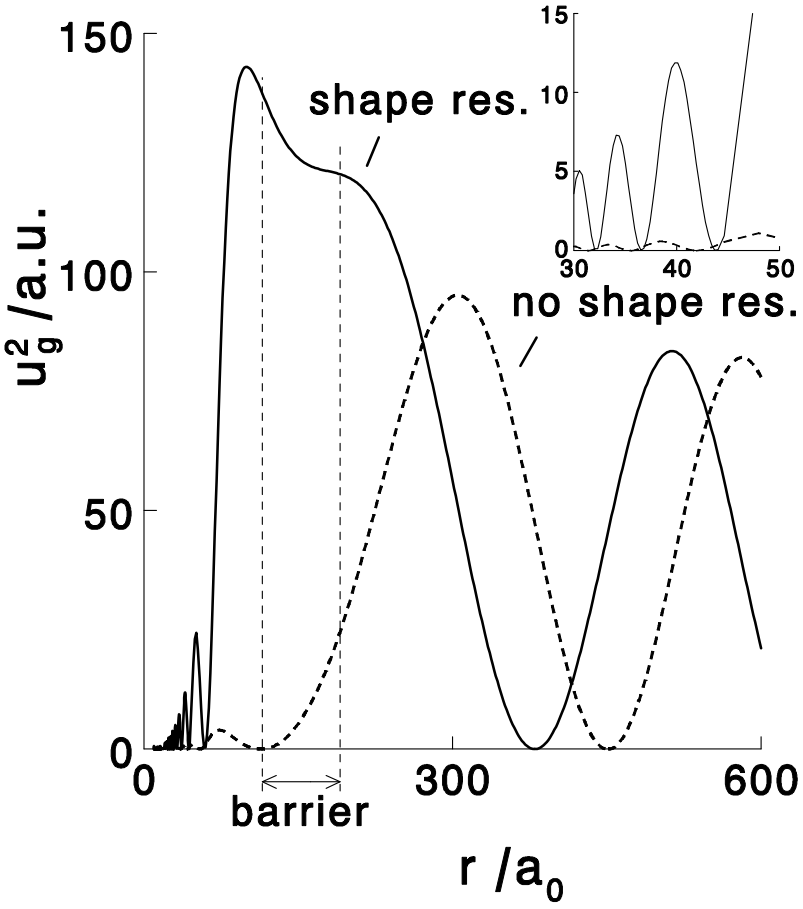


**Figure 4.** Square of $l = 2$ partial-wave ground-state wavefunctions ($^{87}$Rb) $u_g^2(r)$ in the presence of a shape resonance and in the absence of a shape resonance at a collision energy $E = 0.3$ mK. The interatomic distances for which the collision energy is smaller than the potential energy, i.e. for which in a semiclassical picture the atoms tunnel through the barrier, are indicated. Inset, $u_g^2(r)$ in relevant interatomic distance interval for photoassociation. Note the enhancement if a shape resonance is present.

the ground-state potential. It has a dramatic influence on all inelastic processes taking place within the barrier. Figure 4, for instance, shows the radial wavefunction squared for d-wave $^{87}$Rb + $^{87}$Rb scattering in the presence of a shape resonance (the actual situation) and without one. The wavefunction without a shape resonance is calculated by modifying the inner part of the potential slightly so that the shape resonance shifts downward to negative energies. Clearly visible in figure 4 is the phase shift between the wavefunction with and without shape resonance.

Shape resonances are thus expected to tremendously enhance the PA loss rate. The place where this enhancement enters the expressions for the PA loss rate is in the partial width $\gamma_L$ for decay of the PA Feshbach resonance. In turn, it then shows a resonance dependence on the collision energy, as will be described explicitly in the following section.

The existence of a shape resonance in a partial-wave channel leads to the possibility of extracting useful information on cold collisions. Without it, as explained above, the Franck–

Condon oscillations lead to information on the nodes in the radial wavefunction in the excitation region. Translating this to the nodal structure at infinity, i.e. the triplet scattering length, requires sufficiently accurate knowledge of the long-range interaction. For this reason, when extracting a scattering length from the energy dependence of Franck–Condon factors alone, one generally needs to use theoretical information on dispersion coefficients, in particular, the $C_6$ coefficient [10]. The existence of a shape resonance below the top of the barrier yields precisely the second piece of information needed to determine $C_6$ and $a_T$ separately from experiment, essentially because it can also be considered as a function of these two parameters. In [16] we have demonstrated this more explicitly than here (see in particular figure 4 and the corresponding discussion in the text of that paper).

## 3. Determination of excited-state parameters

The expression for the partial width $\gamma_L$ used in our analysis of PA experiments contains a radial transition matrix element with a product of excited and ground-state radial wavefunctions. To calculate the former we need a sufficiently accurate excited-state potential $V_e$. The determination of this potential is not only of interest for this purpose. Investigations of the excited-state potential have led to a very accurate prediction of the excited-state lifetime of optically excited atoms. The possibility of such a prediction arises from the fact that the lifetime contains the same electric-dipole matrix element as that occurring in the $1/r^3$ resonant electric-dipole part of $V_e$.

Existing methods to extract dipole matrix elements from photoassociation spectra are based on a semiclassical approximation [6] or limited by the uncertainty of the inner part of the potential [17]. The $0_g^-$ state asymptotically connecting with the $S_{1/2} + P_{3/2}$ fine-structure limit is an exception to this last statement, because this is a pure long-range state which can entirely be described by a limited set of dispersion coefficients [18–21]. In this section we will present a new approach, based on the accumulated-phase method [10, 22, 23], not limited by any semiclassical approximation or inaccuracy of the inner part of the potential. Again, a brief presentation of this new approach has been given in a previous publication [10]. A recent survey of work on the extraction of accurate predictions of excited atomic state lifetimes from cold-atom PA experiments has been presented by Weiner *et al* [11].

As pointed out above, the excited state we are using in our experiment is the $0_g^-$ state, asymptotically connecting with the $S_{1/2} + P_{1/2}$ state. In the above we have briefly referred to the $2 \times 2$ eigenvalue problem determining the electronic structure of the excited $0_g^-$-states at large interatomic distances. It contains the fine-structure splitting of the excited atom and the interatomic $1/r^3$ resonant dipole interaction. In the fine-structure basis it is given by

$$\begin{aligned} V_{0_g^-} &= \begin{pmatrix} E_{at}(S_{1/2}) + E_{at}(P_{3/2}) & 0 \\ 0 & E_{at}(S_{1/2}) + E_{at}(P_{1/2}) \end{pmatrix} + V_{dd} \\ &= -\frac{1}{4\pi\epsilon_0 r^3} \begin{pmatrix} d(P_{3/2})\, d(P_{3/2}) & \sqrt{2}\, d(P_{1/2})\, d(P_{3/2}) \\ \sqrt{2}\, d(P_{1/2})\, d(P_{3/2}) & 0 \end{pmatrix} + \begin{pmatrix} E_{fs} & 0 \\ 0 & 0 \end{pmatrix} \end{aligned} \tag{2}$$

with $E_{at}$ the energies of the atomic states involved, $V_{dd}$ the resonant electric dipole–dipole part, $E_{fs}$ the fine-structure splitting and $d(P_{1/2})$, $d(P_{3/2})$ the atomic electric-dipole matrix elements, connecting the ground state with the $P_{1/2}$, $P_{3/2}$ excited states. Note that the $^2S_{1/2} + {}^2P_{1/2}$ diagonal matrix element of the $1/r^3$ interaction vanishes because an electronic $j = 0$ state is spherically symmetric, so that there is no preferential orientation of the atomic centres of mass relative to one another. In more formal terms this interaction has the angular momentum

structure proportional to

$$\left[Y_2(\hat{r}), \left(\vec{d}(1), \vec{d}(2)\right)_2\right]_{00} \tag{3}$$

and according to the Wigner–Eckart theorem the expectation value of a rank-2 tensor operator in an angular momentum 0 state is zero. As a consequence, since we are studying photoassociation at interatomic distances for which $E_{\rm fs}$ is much larger than the electric dipole–dipole interaction, the product $d(\mathrm{P}_{1/2})\, d(\mathrm{P}_{3/2})$ is the leading term in the strength of the $1/r^3$ coefficient of the lower $0_{\rm g}^-$ potential. In the following we will use the shorthand notation

$$d^2 = d(\mathrm{P}_{1/2})\, d(\mathrm{P}_{3/2}) \tag{4}$$

for this product.

To justify some aspects of our method we construct a model $0_{\rm g}^-$ potential. For the long-range part we use the dispersion coefficients of Bussery [24] and Gardner *et al* [10]. The inner part is based on a calculation of the eigenvalues of a potential matrix, consisting of the triplet potentials of Spiegelmann *et al* [25] and an $r$-independent fine-structure splitting. The two parts are connected by an exponentially varying exchange term. Using this potential we calculate the phase $\phi_0$ of the rapidly oscillating radial wavefunction at an interatomic distance $r_1 = 30\ a_0$ for the whole range of experimental excited bound-state energies. It turns out that to very good accuracy $\phi_0$ varies linearly over the entire energy range. This implies that

**Table 1.** Positions for experimentally observed bound states $E_J$ of the $^{85}$Rb + $^{85}$Rb and $^{87}$Rb + $^{87}$Rb interatomic potentials, asymptotically connecting with the $S_{1/2}$ + $P_{1/2}$ fine-structure limit. The barycentre of the transition from $^{85}\mathrm{Rb}(2s_{1/2}(F = 3))$ + $^{85}\mathrm{Rb}(2s_{1/2}(F = 3))$ to $^{85}\mathrm{Rb}(2s_{1/2})$ + $^{85}\mathrm{Rb}(2p_{1/2})$ is 12 578.8640 cm$^{-1}$. The barycentre of the transition from $^{87}\mathrm{Rb}(2s_{1/2}(F = 2))$ + $^{87}\mathrm{Rb}(2s_{1/2}(F = 2))$ to $^{87}\mathrm{Rb}(2s_{1/2})$ + $^{87}\mathrm{Rb}(2p_{1/2})$ is 12 578.780 cm$^{-1}$.

| $E_2$ ($^{87}$Rb) (cm$^{-1}$) | $E_2 - E_0$ ($^{87}$Rb) (cm$^{-1}$) |
|---|---|
| 12 576.986 ± 0.003 | |
| 12 575.948 ± 0.003 | |
| 12 575.309 ± 0.003 | |
| 12 572.850 ± 0.003 | 0.123 ± 0.001 |
| 12 571.836 ± 0.003 | 0.132 ± 0.001 |
| 12 570.716 ± 0.003 | |
| 12 569.489 ± 0.003 | |
| 12 568.152 ± 0.003 | |
| 12 566.701 ± 0.003 | |
| $E_0$ ($^{85}$Rb) (cm$^{-1}$) | $E_2 - E_0$ ($^{85}$Rb) (cm$^{-1}$) |
| 12 575.499 ± 0.003 | 0.101 ± 0.001 |
| 12 574.776 ± 0.003 | 0.108 ± 0.001 |
| 12 573.963 ± 0.003 | 0.114 ± 0.001 |
| 12 573.052 ± 0.003 | 0.124 ± 0.001 |
| 12 572.037 ± 0.003 | 0.129 ± 0.001 |
| 12 570.92 ± 0.03 | |
| 12 569.68 ± 0.03 | 0.146 ± 0.001 |
| 12 568.37 ± 0.03 | |
| 12 566.90 ± 0.03 | 0.159 ± 0.001 |
| 12 565.30 ± 0.03 | |
| 12 563.60 ± 0.03 | 0.180 ± 0.001 |
| 12 561.78 ± 0.03 | 0.184 ± 0.001 |
| 12 559.81 ± 0.03 | 0.193 ± 0.001 |
| 12 557.70 ± 0.03 | 0.206 ± 0.001 |

we can summarize the history of the colliding atoms inside $r_1$ in the range of experimental energies entirely with a very limited number of only four parameters: $\phi_0$, its derivative with respect to the bound-state energy $\phi_E$, $d^2$, and the $C_{6e}$ dispersion coefficient. We also include the higher-order dispersion interactions ($C_n/r^n$ with $n > 8$ [24]); the uncertainty in these interactions is not important to the present analysis.

In our analysis we use $J = 0$ levels for $^{85}$Rb and $J = 2$ levels for $^{87}$Rb (see table 1). In the combined analysis of these sets we have only five parameters, because the phase derivatives for the two isotopes can directly be related to each other by a $\sqrt{m}$ scaling rule

$$^{87}\phi_E = \sqrt{\frac{m(^{87}\mathrm{Rb})}{m(^{85}\mathrm{Rb})}}\,{}^{85}\phi_E. \tag{5}$$

Note that $^{87}\phi_0$ and $^{85}\phi_0$ have a similar scaling relationship, but we vary these phases mod $\pi$ independently, because we do not know their integer $\times\pi$ parts. We now calculate for each set of these parameters the corresponding bound-state energies and construct a $\chi^2$-function

$$\chi^2 = \sum_i \left( \frac{E_{\mathrm{exp},i} - E_{\mathrm{th},i}(^{85}\phi_0, {}^{87}\phi_0, {}^{85}\phi_E, C_{6e}, d^2)}{\sigma_{E_{\mathrm{exp},i}}} \right)^2 \tag{6}$$

where $E_{\mathrm{exp},i}$ are the experimental bound-state energy levels, $E_{\mathrm{th},i}$ the theoretically calculated ones and $\sigma_{E_{\mathrm{exp},i}}$ the standard deviation in the experimental level $i$. In figure 5 the area in the $C_{6e}$, $d^2$-plane is shown where $\chi^2$ is minimal or at most equal to twice the minimum value, for the optimum values of the three phase parameters. This condition clearly defines a strip in the $C_{6e}$, $d^2$-plane with a width of 0.2 au in the $d^2$-direction. Using the theoretical $C_{6e}$ value from [24] we find $d^2 = 8.8 \pm 0.1$ au, in good agreement with a recent value measured by beam-gas-laser spectroscopy [26].

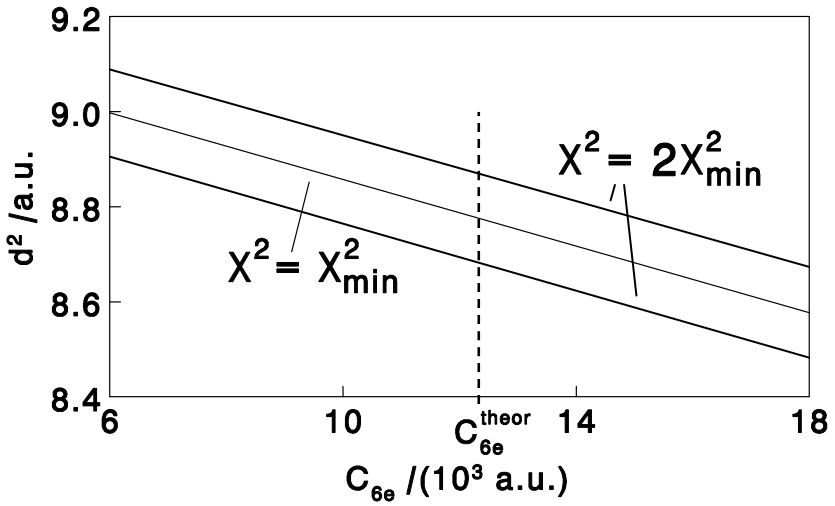


**Figure 5.** Contour plot of $\chi^2$ as a function of $C_{6e}$ and $d^2$ for the optimum values of the three phase parameters. The broken vertical line indicates the theoretical value ($C_{6e}^{\mathrm{theor}}$) of [24].

## 4. Decay mechanisms of the $^{85}$Rb g-wave shape resonance

### *4.1. Introduction*

In the above we considered the decay of the shape resonance by PA laser excitation. Also, other decay processes become important if the lifetime of the shape resonance is comparable to or longer than the time scale for these decay mechanisms. In this section we consider inelastic scattering mechanisms due to decay to other ground-state hyperfine channels. As pointed out in the brief first report on our work [14], long-lived shape resonances lend themselves to a new kind of sensitive study of such processes. In this connection there is special interest in so-called second-order spin–orbit coupling $V_{\rm so}^{(2)}$, or indirect spin–spin interaction, which arises from a mechanism very similar to the magnetic dipolar interaction $V_{\rm dip}$ between the valence electron spins, the only difference being that it does not mediate directly through a magnetic field but via the electric field from the charges in the system†. Recently, an *ab initio* calculation of $V_{\rm so}^{(2)}$ was presented [29] for various alkali atoms, in particular $^{87}$Rb. For low molecular states expectation values have been measured as well as calculated [28], but these give information on small internuclear distances only.

Three mechanisms compete in depleting the shape resonance: the inelastic decay with rate constant $\gamma_{\rm inel}/\hbar$ due to coherent contributions from dipolar decay and spin–orbit decay: $\gamma_{\rm inel} = (\sqrt{\gamma_{\rm dip}} + \sqrt{\gamma_{\rm so}})^2$, the tunnelling rate ($\gamma_{\rm out}/\hbar$) and the excitation to the excited state via photoassociation ($\gamma_{\rm L}/\hbar$). Note that scattering theory [15] shows that the partial-wave amplitudes, denoted above as $\sqrt{\gamma_{\rm dip}}$ and $\sqrt{\gamma_{\rm so}}$, are (positive or negative) real quantities. All these quantities hinge critically on the exact energy $E_{\rm res}$ of the shape resonance, which is subject to a large uncertainty even if we know that it exists below the top of the centrifugal barrier. Knowing the energy of this resonant state is comparable to knowing the last bound state energy of a potential [30] and thus is important in determining the scattering length, which is of great relevance for Bose–Einstein condensation experiments.

To determine $E_{\rm res}$ and $\gamma_{\rm inel}$, in particular its $\gamma_{\rm so}$ part, from experiment we have performed a simultaneous analysis of time-dependent photoassociation data at high laser power, thus eliminating complicated cross-terms between $\gamma_{\rm inel}$ coupling and laser coupling during the photoassociation pulses, and time-independent photoassociation data at very low laser intensity, for which the laser excitation can be treated in first order. To study the influence of $\gamma_{\rm inel}$ on the photoassociative losses at low laser intensities we have to include its influence in the PA loss rate. This will be done in the following part of this section. In the last part we will discuss the analysis of the time-dependent data and the determination of $E_{\rm res}$ and $\gamma_{\rm so}$.

### *4.2. Photoassociation rate constant including inelastic decay*

To first order in the laser intensity, the squared scattering $S$-matrix element describing the single-atom optical excitation for a pair of colliding ground-state atoms with collision energy $\epsilon$ and the subsequent spontaneous decay (decay rate $\gamma_0/\hbar$), using a photoassociation laser with frequency $\omega_{\rm L}$ and field strength $\vec{E}_{\rm L} = E_{\rm L}\vec{\sigma}_{\rm L}$, can be written as

$$|S_{\rm PA}|^2 = \frac{\gamma_0\gamma_{\rm L}(SM_S lm_l, \epsilon \to \Omega JM)}{(\epsilon + E_{\rm g} + \hbar\omega_{\rm L} - E_{\rm e})^2 + \gamma_0^2/4}. \tag{7}$$

† This interaction was first studied by [27]. Its importance for the properties of ultracold alkali gases was first pointed out by P Julienne *et al*. A detailed treatment can be found in [28].

In this expression the previously mentioned partial width $\gamma_L$ for excitation of an $|SM_S lm_l, \epsilon\rangle$ ground state to an $|\Omega J M\rangle$ excited state is equal to

$$\gamma_L = 2\pi \left|\langle \Omega J M | \left[\vec{d}(1) + \vec{d}(2)\right] \cdot \vec{E}_L | SM_S lm_l, \epsilon\rangle\right|^2. \tag{8}$$

In equations (7) and (8) $E_e$ is the excited rovibrational state energy, $E_g$ the asymptotic internal energy in the ground-state channel, $\vec{d}(i)$ the electric dipole operator of atom $i$, $\Omega$ the total electronic magnetic quantum number along the internuclear axis $z'$ and $J$, $M$ the total molecular angular momentum quantum numbers, excluding the nuclear spins.

From $|S_{PA}|^2$ we obtain the photoassociation rate constant $K(T, \omega_L)$ for a gas of cold atoms with temperature $T$ by calculating a thermal average

$$K(T, \omega_L) = \left\langle v \frac{\pi}{k^2} |S_{PA}|^2 \right\rangle_{th}. \tag{9}$$

For our purposes the most important factor in this rate constant is the partial width $\gamma_L$, which will be worked out in more detail in the following paragraphs.

We expand the excited-state $|\Omega J M\rangle$ in products of atomic fine-structure states with a well defined electronic angular momentum $j, m_j$:

$$\begin{aligned} |\Omega J M\rangle &= \sum_j c_j(r) |j \Omega J M\rangle \\ &= \sum_j c_j(r) \sum_l (-1)^{j-\Omega} (J\Omega j - \Omega | l0) | j l J M\rangle \\ &= \sum_{j m_j l m_l} c_j(r) (-1)^{j-\Omega} (J\Omega j - \Omega | l0)(j m_j l m_l | J M) | j m_j l m_l\rangle. \end{aligned} \tag{10}$$

Substituting this in equation (8) leads to

$$\gamma_L = \frac{2\pi I_L}{\epsilon_0 c} \left| \sum_{j m_j} (-1)^{j-\Omega} (J\Omega j - \Omega | l0)(j m_j l m_l | J M) \int_0^\infty \mathrm{d}r\, c_j(r)\, u_{\Omega J}(r) \right.$$
$$\left. \times \langle j m_j | \left[\vec{d}(1) + \vec{d}(2)\right] \cdot \vec{\sigma}_L | S M_S\rangle u_{S M_S l m_l, \epsilon}(r) \right|^2 \tag{11}$$

containing the Franck–Condon overlap integral between the ground- and excited-state radial wavefunctions $u_{SM_S lm_l,\epsilon}(r)$ and $u_{\Omega J}(r)$, respectively. A shape resonance in the ground-state channel causes the initial radial wavefunction and thus $\gamma_L$ to show resonance behaviour. We again refer to figure 4 demonstrating the strong enhancement.

Note that by the above substitution of equation (10) in equation (8) an additional independent summation over $l, m_l$ quantum numbers of the final state would, in principle, appear. Since the quantum numbers of the initial state stand only for the asymptotic incoming spherical wave part, which may be different from the additional partial waves introduced into the initial state by inelastic interactions, one will in general have incoherent contributions for various final choices of these quantum numbers. This freedom should, in principle, be allowed for, once one is to include inelastic ground-state contributions that change the relative orbital angular momentum, such as the direct and indirect spin–spin coupling. This is what we are now going to consider.

A straightforward but laborious method to include the influence of inelastic scattering on the shape resonance would be to replace the simple initial state in equation (11) by a coupled-channels wavefunction. This would automatically include combined effects from the shape resonance and the inelastic ground-state transitions. Concentrating on the g-wave shape resonance, a calculation of the coupled-channels state for the nine incoming $m_l$ spherical waves,

for a large set of collision energies, and for the large number of inelastic hyperfine channels would be very laborious. Fortunately, we were able to show that a much simpler approach is possible, by comparing a few representative coupled-channel wavefunctions inside the barrier (the only positions where they enter the Franck–Condon integral) for a ground-state model potential, with and without the inclusion of the inelastic spin–spin terms. Like the model potential for the $0_g^-$ state, this model potential is only introduced for the purpose of studying the general properties of the corresponding wavefunctions.

The Hamiltonian of the coupled-channel ground-state problem is of the form

$$H = T + V_c + V_{hf} + V_Z + V_{dip} + V_{so}^{(2)} \tag{12}$$

a sum of a kinetic energy operator $T$, the central interaction $V_c$, a sum of single-atom hyperfine interactions $V_{hf}$, the Zeeman interaction $V_Z$, the magnetic dipolar interaction $V_{dip}$ and the second-order spin–orbit interaction $V_{so}^{(2)}$. A test coupled-channels calculation shows that the exact radial location and shape of $V_{so}^{(2)}$ are irrelevant. The only relevant quantity is the area $\bar{V}_{so}^{(2)}$ of the radial profile, since in the radial transition integral the elastic wavefunctions are virtually identical and oscillate so rapidly at the interatomic distances where $V_{so}^{(2)}$ is effective that only the above area multiplied by the elastic amplitude squared is of importance. The central interaction $V_c$ is only partially known. The long-range part of the triplet potential and associated partial-wave radial wavefunctions for $r > 35\,a_0$ follow from our previous analyses of photoassociation spectra [10, 14, 16]. At these distances they can be described by a $C_6$-tail and an asymptotic behaviour dictated by the triplet scattering length. For the inner part we use the theoretical potential of Krauss and Stevens [31]. We take the singlet potential from Amiot [32] and the above-mentioned $C_6$ value for the tail. Finally, to vary the unknown singlet scattering length we add a variable phase to the singlet radial wavefunctions at small interatomic distances.

Without the inelastic spin–spin terms the shape resonance can only decay via tunnelling through the centrifugal barrier. This implies that the initial state $|SM_S lm_l, \epsilon\rangle$ in equation (8) contains only the single partial-wave radial wavefunction $u_{SM_S lm_l,\epsilon}(r)$. Calculating this wavefunction at a fixed arbitrary radius $r_1$ inside the barrier, we find that its dependence on the collision energy can be very accurately described by a factor

$$\frac{\sqrt{E}^{\,l+1/2}}{E - E_{res} + i\gamma_{out}/2} \tag{13}$$

with $l = 4$ for the shape resonance. This expression follows from Wigner's threshold law in combination with the theory of resonances in scattering processes [33]. For the energy range where the resonance energy $E_{res}$ is expected to occur the tunnelling width $\gamma_{out}$ of the resonance agrees very well with the semiclassical value.

We now proceed by adding the direct and indirect spin–spin terms $V_{dip}$ and $V_{so}^{(2)}$ to the Hamiltonian. We then also find inelastic hyperfine components of the initial state, which make it necessary to extend equation (8) for $\gamma_L$ by adding total two-atom nuclear spin quantum numbers $I, M_I$ to the final state and summing incoherently over their values. We stress again that the nuclear spins are decoupled in the final state. Also the asymptotic incoming quantum numbers of the initial state have to be supplemented with $I, M_I$ values. To keep the discussion transparent we now add a superscript '0' to the quantum numbers of the elastic component of the initial state, to distinguish them from values for the inelastic components. Because of the choice of a fully spin-stretched initial spin state we have the restriction $S^0 = 1$, $M_S^0 = +1$, $I^0 = 5$, $M_I^0 = +5$, $l^0 = 4$. Note that for this doubly polarized situation we also have $f_1^0 = 3$, $f_2^0 = 3$, $F^0 = 6$, $M_F^0 = +6$. The initial states differ only in the value of $m_l^0$, which varies from $-4$ to $+4$. For each of these initial states the ground-state coupled-channels calculation leads to the addition of a superposition of inelastic components.

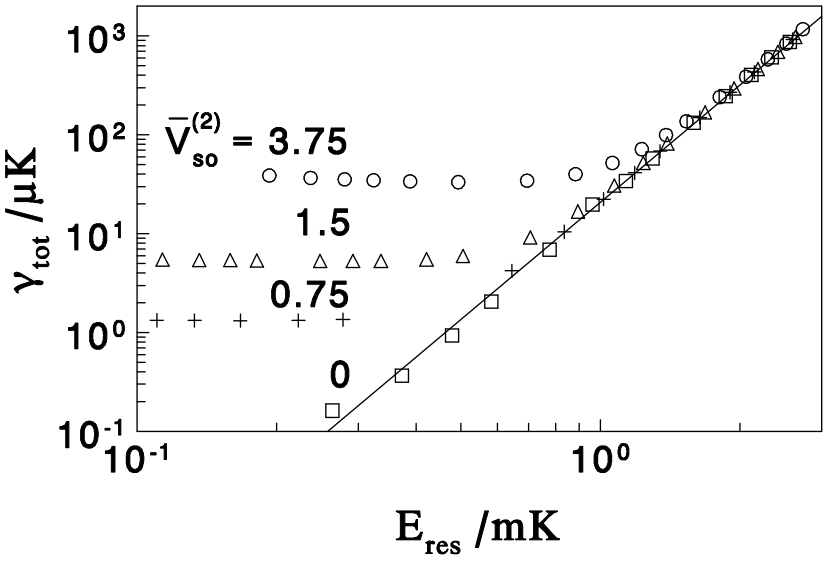


**Figure 6.** Total width $\gamma_{\rm tot} = \gamma_{\rm out} + \left(\sqrt{\gamma_{\rm dip}} + \sqrt{\gamma_{\rm so}}\right)^2$ of the elastic wavefunction as a function of the resonance energy for various $\bar{V}^{(2)}_{\rm so}$ values (in K$a_0$) following from CC calculations. The straight line shows the tunnelling width ($\gamma_{\rm out} \sim E^{4.5}$).

It turns out that the complicated coupled-channel superpositions can be calculated to very high accuracy by a simple approach, in which one calculates the influence of the inelastic interactions on the original shape resonance state by perturbation theory. This leads to a splitting into a set of shape resonance states with resonance energies and widths changed by $\Delta E_{\rm res}$ and $\Delta\gamma$. A detailed study shows that each $\Delta E_{\rm res}$ varies linearly with the unknown strength of $V^{(2)}_{\rm so}$ for reasonable strengths, just as expected from first-order time-independent perturbation theory. The total width of each of the split resonances turns out to be equal to the (incoherent) sum of the tunnelling width $\gamma_{\rm out}$ and a contribution from coherent direct and indirect spin–spin terms:

$$\gamma_{\rm tot} = \gamma_{\rm out} + \Delta\gamma \qquad \Delta\gamma \equiv \gamma_{\rm inel} = \left(\sqrt{\gamma_{\rm dip}} + \sqrt{\gamma_{\rm so}}\right)^2. \tag{14}$$

Figure 6 illustrates this result. In the $\bar{V}^{(2)}_{\rm so}$ range considered, $\Delta\gamma$ varies quadratically with the strength of $V^{(2)}_{\rm so}$, as expected from first-order time-dependent perturbation theory. It should be pointed out that the dipolar interaction already leads to similar changes by itself.

Our simple approach consists of calculating the shifts $\Delta E_{\rm res}$ by including a limited number of inelastic hyperfine channels that are significantly coupled in. The appropriate basis to discuss this point is the hyperfine basis $|(f_1 f_2)FM_F\rangle$. It turns out that of all possible components allowed by the selection rules only a very limited number contribute significantly to $\gamma_{\rm L}$: those that are enhanced by the existence of the shape resonance, are sufficiently close in energy and are coupled in via significant matrix elements. Since the hyperfine splitting is very large compared to the inelastic interaction strengths, the coupling between the three $f_1$, $f_2$ subspaces can be neglected. We restrict ourselves to the $f_1 = 3$, $f_2 = 3$ subspace, because it contains the incoming fully spin-stretched state. As a consequence, the operators $V_{\rm hf}$, $V_{\rm Z}$, $V_{\rm dip}$ and $V^{(2)}_{\rm so}$ are equivalent to simpler effective operators: $V_{\rm hf}$ becomes a constant, $V_{\rm Z}$ couples the $z$-components $f_{1z}$ and $f_{2z}$ with effective gyromagnetic ratios

$$\gamma_f = (\gamma_{\rm e} s - \gamma_n i)/f = \gamma_{\rm e}/6 - 5\gamma_n/6 \tag{15}$$

to the field instead of the electronic and nuclear spins separately, $V_{\rm dip}$ as well as $V_{\rm so}^{(2)}$ couple $\vec{f}_1$ and $\vec{f}_2$, instead of $\vec{s}_1$ and $\vec{s}_2$.

The picture thus following from our coupled-channel calculations is that of a new spectroscopy of long-lived states of two atoms inside a barrier, the structure of which follows from the competition between the mutual spin–spin interaction, coupling $\vec{f}_1$ with $\vec{f}_2$, and the Zeeman precession. A fascinating aspect is the weakness of the effective spin–spin interaction: taking into account the available volume inside the barrier it is only of the order of 0.02 mK. The field strength needed to break it is only of order 0.2 G. With an actual field of only 7 G we are already in the strong-field limit. Although the radial dependences of $V_{\rm so}^{(2)}$ and $V_{\rm dip}$ are highly different, they operate spatially only via the expectation values of their radial parts. The problem is therefore completely equivalent to that of two magnetic dipoles with the orientation-dependent interaction

$$V_{\rm spin\text{–}spin} = V_{\rm dip} + V_{\rm so}^{(2)} = (a_{\rm dip} + a_{\rm so})\left[\vec{f}_1 \cdot \vec{f}_2 - 3(\hat{r} \cdot \vec{f}_1)(\hat{r} \cdot \vec{f}_2)\right] \tag{16}$$

confined to move inside a barrier. Including the angular degrees of freedom, the eigenstates labelled $i$ are superpositions of basis states:

$$\sum_{m_l} \alpha_{i,m_l} |(f_1 f_2) F M_F l m_l\rangle \tag{17}$$

with $f_1 = f_2 = 3$, subject to the selection rule $M_F + m_l = 6 + m_l^0$.

For the special case of the incident value $m_l^0 = +4$, for instance, the solution is very simple. In that case we have an elastic wavefunction component only, which differs, however, from that without inelastic interactions. It again shows a resonance behaviour as a function of collision energy (see figure 7), but with the original Breit–Wigner resonance denominator of equation (13) replaced by one with modified $E_{\rm res}$ and $\gamma$, as indicated above. Apart from this replacement, there is to very good accuracy no change in the elastic wavefunction.

For $m_l^0 = +3$ the situation becomes more complicated. The number of coupled components increases from nine ($m_l^0 = +4$) to 16. The two significantly coupled states, $f_1 = 3, f_2 = 3, F = 5, M_F = +5, l = 4, m_l = +3$ and $f_1 = 3, f_2 = 3, F = 5, M_F = +4, l = 4, m_l = +4$, degenerate without Zeeman and inelastic interactions. For $B \gg 0.2$ G this degeneracy is first lifted by the Zeeman interaction. Subsequently considering $V_{\rm dip}$ and $V_{\rm so}^{(2)}$ as first-order perturbations we thus find the energy shifts for the split shape resonance states. Figure 8 shows a comparison between energy shifts following from coupled-channel calculations and values from this simple first-order perturbation treatment in which only $\bar{V}_{\rm so}^{(2)}$ occurs as a parameter. Clearly, the first-order perturbation treatment describes the rigorous coupled-channel results very well. The same conclusion holds for lower $m_l^0$ values and other $B$-values ($\gg 0.2$ G).

Also, the widths of the new shape resonance states can be described with a perturbation treatment. In this case the lower $f_1$, $f_2$ hyperfine subspaces cannot be left out: the large final available phase space leads to large contributions to the total decay width. The total inelastic width of the resonant state is a sum of partial widths for decay to all possible hyperfine channels. Each width contains a radial transition matrix element of the sum of $V_{\rm so}^{(2)}$ and $V_{\rm dip}$ between the wavefunctions before and after decay, to which the earlier remark about the area of the radial profile of $V_{\rm so}^{(2)}$ applies. Making use of some Clebsch–Gordan algebra, we can express the total set of decay matrix elements and thus the total change of the width for all $m_l^0$ and $B$ values in terms of the same unknown constant $\bar{V}_{\rm so}^{(2)}$.

Only one aspect needs to be discussed before finishing the presentation of the simple approach. As pointed out above, for $m_l^0 = 4$ there is only one channel involved. The replacement of the unperturbed Breit–Wigner denominator by a perturbed one is then equivalent

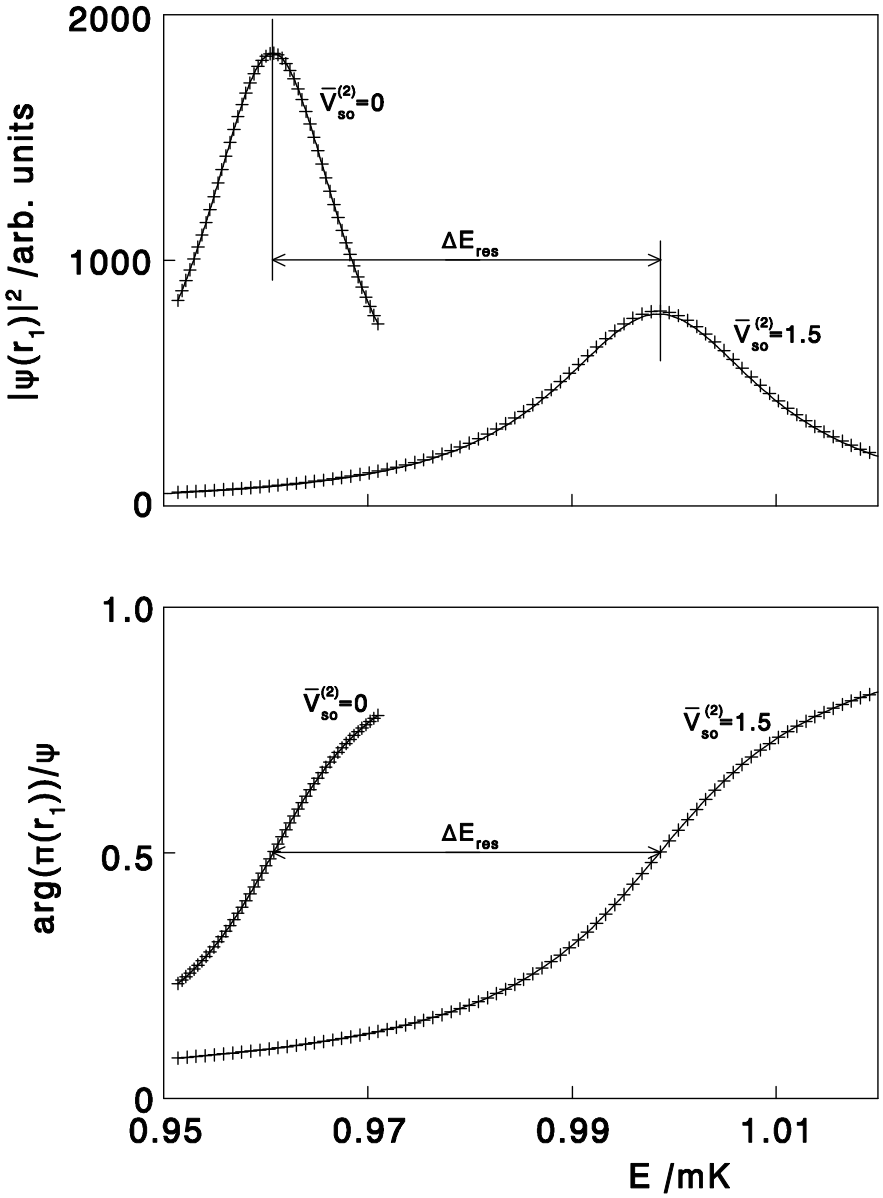


**Figure 7.** Square (*a*) and argument (*b*) of the elastic ground-state wavefunction at $r_1 = 45\ a_0$ as a function of collision energy for $\bar{V}_{so}^{(2)} = 0$ and $\bar{V}_{so}^{(2)} = 1.5\ \mathrm{k}a_0$. The wavefunctions are corrected for the background behaviour $E^{4.5}$. The crosses are CC results, the lines show the result of the resonance formula, in the case $\bar{V}_{so}^{(2)} = 1.5\ \mathrm{K}a_0$ with $E_{res} = 1.00$ mK and $\gamma_{tot} = \Delta\gamma + \gamma_{out} = 25.4\ \mu$K. The energy shift due to $V_{so}^{(2)}$ is indicated by $\Delta E_{res}$.

to a simple multiplication of the total unperturbed state in equations (8) and (11) by the ratio

$$\frac{E - E_{res} + i\gamma_{out}/2}{E - (E_{res} + \Delta E_{res}) + i(\gamma_{out} + \Delta\gamma)/2}. \tag{18}$$

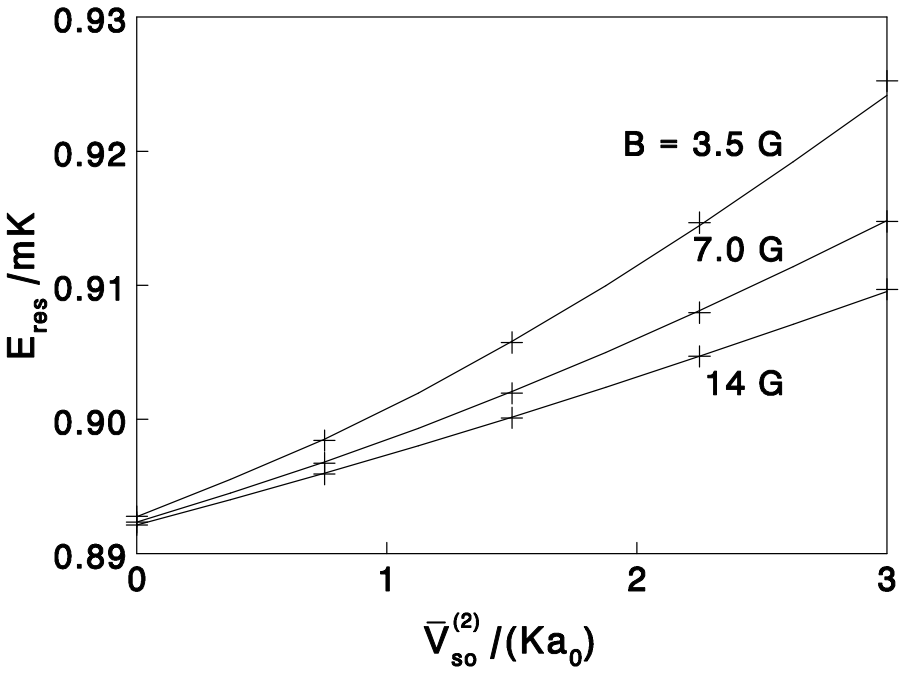


**Figure 8.** Position of a resonant level as a function of $\bar{V}^{(2)}_{\rm so}$ for the $m_l = 3$ entrance channel for various magnetic fields. In the absence of $V^{(2)}_{\rm so}$ and $V_{\rm dip}$ the resonance occurs at $E_{\rm res} = 0.889$ mK. The pluses are CC results, the curves are based on a first-order perturbation model. The energy shift of the resonant level due to $V_{\rm dip}$ alone is 3 $\mu$K.

For lower $m_l^0$ values the situation is more complicated. In that case the perturbed shape resonance states $i$ are superpositions of unperturbed states with coefficients $\alpha_{i,m_l}$, distinguishing the latter states by the quantum number $m_l$. We then need to multiply the unperturbed elastic scattering wavefunction by

$$\sum_i \alpha_{i,m_l} \frac{E - E_{\rm res} + {\rm i}\gamma_{\rm out}/2}{E - (E_{\rm res} + \Delta E^i_{\rm res}) + {\rm i}(\gamma_{\rm out} + \Delta\gamma^i)/2}. \tag{19}$$

In other words, the coefficients $\alpha$ also play the role of determining the amplitudes by which an incoming channel excites the various perturbed shape resonances. This is a direct consequence of Feshbach's reaction theory for overlapping resonances (see [15], p 220). The expressions (18) and (19) have been confirmed by coupled-channel calculations.

Comparing the ratio of theoretical $J = 4$ and 0 or 2 peak areas to the corresponding experimental values *without inelastic decay*, we find the theoretical ratio to be too large. This is an anomaly of the $J = 4$ PA peak that we find in addition to the anomalous features of this peak associated with the shape resonance phenomenon mentioned in section 1. The theoretical $J = 4$ peak area is suppressed by the above replacement of Breit–Wigner denominators. This point is further discussed in [14].

### *4.3. Time-dependent photoassociation spectroscopy*

In the previous sections we have studied a limiting situation of very low laser intensities for which the analysis of the $J = 4$ peak became feasible. This analysis contains only two unknown parameters: the resonance energy $E_{\rm res}$ of the unperturbed shape resonance and

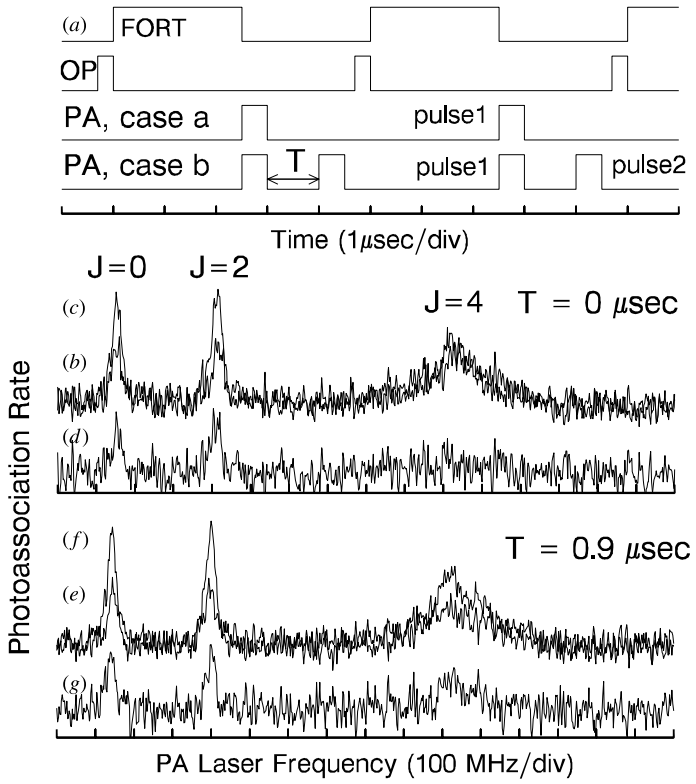


**Figure 9.** (*a*) Timing of laser pulses in the time-dependent photoassociation experiment. (*b*)–(*g*) Spectra of the $0_g^-$ vibrational level at 12 573.04 $cm^{-1}$ for $T = 0$ ((*b*)–(*d*)) and $T = 0.9$ $\mu$s ((*e*)–(*g*)). (*b*), (*e*) Spectrum with one photoassociation pulse only; (*c*), (*f*) spectrum with two photoassociation pulses. (*d*), (*g*) Difference spectra showing the effect of pulse 2 alone, for $T = 0$ and 0.9 $\mu$s, respectively.

the constant $\bar{V}_{so}^{(2)}$. Instead of the latter we choose the related inelastic width $\gamma_{inel}^0 \equiv \Delta\gamma$ for the fully aligned state $m_l^0 = +4$, $m_F = +6$ as a parameter. The resonance energy enters equations (18) and (19) both explicitly and implicitly, i.e. via the tunnelling rate $\gamma_{out}$. By far the most sensitive dependence on $E_{res}$ occurs via $\gamma_{out}$, the exponential energy dependence of a tunnelling rate well known from alpha decay. It appears from our time-independent analysis that it is impossible to determine $\gamma_{out}$ (and therefore $E_{res}$) and $\gamma_{inel}^0$ separately from time-independent data alone. This is clear from equation (18), which shows that the perturbed elastic scattering wavefunction for $m_l^0 = 4$ contains only the sum $\gamma_{out} + \gamma_{inel}^0$. Equation (19) makes clear that for $m_l^0 < 4$ also other linear combinations of these quantities are involved. It turns out, however, that only a relation between these widths can be extracted from the time-independent data. Also, we find that these data are consistent with the theory only for a certain range of ratios $\gamma_{out}/\gamma_{inel}^0 = 2 \pm 1$. In total, the time-independent data do not lead to a unique combination of $\gamma_{out}$ and $\gamma_{inel}^0$.

A completely new, time-dependent photoassociation experiment, however, does give complementary information about $E_{res}$ and $\gamma_{inel}^0$ and also shows direct evidence for the existence of a shape resonance within the $l = 4$ ground-state barrier. A more extensive description of the experimental aspects can be found in [14]. The basic idea (see figure 9) is that the time

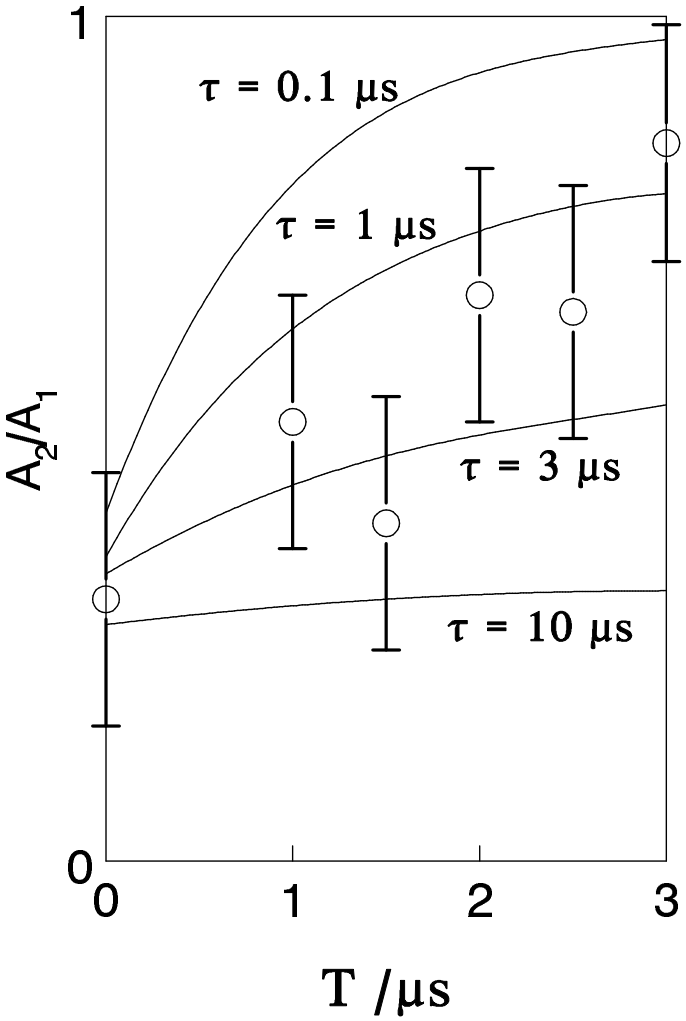


**Figure 10.** Time-dependent signal $A_2/A_1$ as a function of delay time $T$ for $I = 50$ W cm$^{-2}$, $T = 0.35$ mK and $\gamma_{out}/\gamma_{so} = 2$. Experimental data with error bars are indicated as well as theoretical curves for various lifetimes of the shape resonance $\tau$.

period, during which the (FORT) trapping and the optical pumping lasers are switched off, is used for a pulse sequence consisting of either a single photoassociation pulse (experiment (*a*)) or a set of two pulses separated by a delay time $T$ (experiment (*b*)). The PA laser is tuned in such a way that only atoms within the barrier are excited. If the PA laser intensity is chosen to be so high that the first pulse in experiment (*b*) excites all atoms within the barrier, the loss rate due to the second pulse is a measure for the build-up of the resonance state through the barrier during the delay time $T$ and thus also a measure for the lifetime $\tau$ of the resonance in the absence of laser light. Comparing losses in experiments (*a*) and (*b*) then enables us to determine $\tau$. If $T \gg \tau$ the loss in experiment (*b*) will be twice as high as in experiment (*a*), while if $T \ll \tau$ the two loss rates will be equal. This time-dependent effect is directly visible in the experimental spectra in figure 9 and in figure 10. Figure 10 shows the time-dependent signal $A_2/A_1$: the total loss $A_2$ due to the set of second pulses only (area of $J = 4$ peak in the

difference spectrum), divided by the total loss $A_1$ due to the set of single laser pulses per cycle (area of $J = 4$ peak in case (*a*)), as a function of the delay time.

In the model we construct to analyse the time-dependent photoassociation data we divide the trapped atoms into two classes: $N_{\rm in}$, the number of atoms within the $l = 4$ ground-state centrifugal barrier, and $N_{\rm out}$, the number of atoms outside the barrier. The rate equations governing the evolution of these numbers are

$$\frac{{\rm d}N_{\rm in}}{{\rm d}t} = -\left\{\gamma_{\rm L,sp}/\hbar + \gamma_{\rm out}/\hbar + \gamma_{\rm inel}/\hbar\right\} N_{\rm in} + (\gamma_{\rm in}/\hbar)N_{\rm out} \tag{20}$$

$$\frac{{\rm d}N_{\rm out}}{{\rm d}t} = -(\gamma_{\rm in}/\hbar)N_{\rm out} + (\gamma_{\rm out}/\hbar)N_{\rm in} \tag{21}$$

where $\gamma_{\rm L,sp}$ is the partial width of the shape resonance for laser excitation to a bound excited state followed by spontaneous emission, $\gamma_{\rm out}$ ($\gamma_{\rm in}$) the partial width for tunnelling outward (inward) through the barrier, and $\gamma_{\rm inel}$ the partial width for inelastic decay to lower ground-state hyperfine levels, related to $\gamma_{\rm dip}$ and $\gamma_{\rm so}$ as previously indicated. In principle, the quantities $\gamma_{\rm inel}$, $\gamma_{\rm out}$ and $\gamma_{\rm in}$ depend on $m_l^0$. Coupled-channel calculations (as discussed in section 4.2) show that this dependence is weak: the variation over $m_l^0$ is about $\pm 15\%$ for $\gamma_{\rm inel}$ and smaller than $\pm 3\%$ for $\gamma_{\rm out} = \gamma_{\rm in}$. In our analysis we treat the coefficients $\gamma_{\rm inel}$, $\gamma_{\rm out}$ and $\gamma_{\rm in}$ in equations (20) and (21) as average values.

A complication in solving these equations is that saturation effects need to be taken into account in $\gamma_{\rm in}$ and $\gamma_{\rm out}$ (due to changes of $E_{\rm res}$), and in $\gamma_{\rm L,sp}$. To study these effects we have constructed a two-state coupled-channels program with a triplet ground state ($|g\rangle$) and a $0_{\rm g}^-$ excited state ($|e\rangle$), including an imaginary potential term to describe flux loss due to spontaneous emission. Using this program we calculate the probability $1 - |S_{\rm el}|^2$ for escape from the elastic channel, with $S_{\rm el}$ the elastic $S$-matrix element, as a function of the collision energy. For low laser intensities we reproduce equation (7), making use of the unitarity relation

$$|S_{\rm el}|^2 + |S_{\rm PA}|^2 = 1. \tag{22}$$

For high laser intensities we can directly determine $\gamma_{\rm L,sp}$, $\gamma_{\rm out}$ and $E_{\rm res}$ from the escape probability equation for a doorway state

$$1 - |S_{\rm el}|^2 = \frac{\gamma_{\rm out}\gamma_{\rm L,sp}}{(E - E_{\rm res})^2 + \frac{1}{4}(\gamma_{\rm out} + \gamma_{\rm L,sp})^2} \tag{23}$$

considering the shape resonance as a doorway state that the system has to pass through to enter the excited state (see [15], p 179). In figure 11 these quantities are shown as a function of the laser detuning. In this figure the laser detuning is given with respect to the energy difference of the bound excited level and the shape resonance level. For vanishing laser detuning relative to the molecular transition frequency, we find $\gamma_{\rm out}$ to be reduced by a factor of 2 with respect to the corresponding semiclassical value. This is due to the fact that the laser coupling is so strong that the tunnelling process cannot be discussed in terms of the bare states $|g\rangle$ and $|e\rangle$. Instead, the dressed states $|1N\rangle = (|g, N+1\rangle + |e, N\rangle)/\sqrt{2}$ and $|2N\rangle = (|g, N+1\rangle - |e, N\rangle)/\sqrt{2}$ have to be used [34].

The rate constants $\gamma_{\rm L,sp}$, $\gamma_{\rm in}$ and $\gamma_{\rm out}$, obtained in this way, can be used for solving equations (20) and (21). The calculated loss rates can be compared directly with the corresponding experimental quantities. In figure 10 the ratio of the loss $A_2$ due to the second pulse in experiment (*b*) alone and the loss $A_1$ due to the pulse in experiment (*a*) is compared with the corresponding theoretical ratio for $\gamma_{\rm out}/\gamma_{\rm inel} = 2$. For a discussion of the consequences of this result for $\gamma_{\rm so}$ and the indirect spin–spin relaxation of a $^{87}$Rb condensate, we refer to [14].

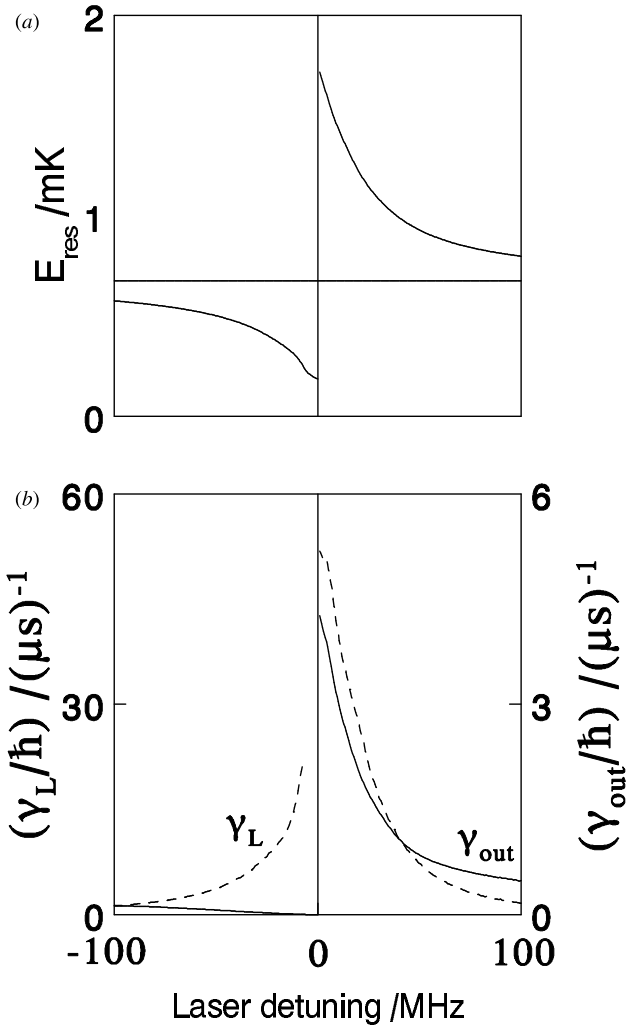


**Figure 11.** (*a*) g-wave resonance energy; (*b*) $\gamma_{\rm out}$ (full curve) and $\gamma_{\rm L,sp}$ (broken curve) as a function of laser detuning for $I = 48$ W cm$^{-2}$.

In connection with the present work we have to address the question of whether the above-mentioned conclusions concerning the role of $V_{\rm so}^{(2)}$ in the photoassociation process for $^{85}$Rb affect the results of [16] for $^{87}$Rb. An analysis along the lines of the present work for $^{87}$Rb shows that the tunnelling lifetime of the d-wave shape resonance in this case is much shorter than $\gamma_{\rm inel}$, justifying the earlier analysis in which we neglected the spin–orbit (and dipolar) relaxation of the shape resonance.

## 5. Conclusion

We have described methods to extract information on interactions between ultra-cold atoms from photoassociation experiments. We were able to find experimental circumstances where this is relatively easy. These circumstances include: (*a*) the selection of the doubly polarized

state for the colliding atoms and (*b*) the selection of the lower $0_g^-$ state as the excited electronic state, leading to a Hund's (e) case as the prevailing coupling scheme. The advantages of this choice of circumstances are that the photoassociation process maps out the radial dependence of the collisional wavefunction and its overall magnitude for a single partial wave.

We have also presented a method for the determination of excited-state parameters and finally we have explored a possibility to explain the anomalous features of observed $J = 4$ photoassociation peaks in terms of a system of two atoms moving inside a centrifugal barrier under the influence of the mutual spin–spin interaction of the dipolar and the spin–orbit type. We have shown how to combine information from a time-independent photoassociation experiment with that from a pulsed photoassociation process to confirm our explanation and to extract additional properties of the g-wave shape resonance. The emphasis in the present paper has been on a more complete presentation of the methods used in our previous brief publication [14]. The final results are the same as presented in that paper.

## Acknowledgments

Work at the University of Texas was supported by the R A Welch Foundation, the National Science Foundation, and the NASA Microgravity Science and Applications Research Division.

## References

[1] Gibble K and Chu S 1992 *Metrologia* **29** 201
[2] Anderson M H, Ensher J R, Matthews M R, Wieman C E and Cornell E A 1995 *Science* **269** 198
[3] Bradley C C, Sacket C A, Tollet J J and Hulet R G 1995 *Phys. Rev. Lett.* **75** 1687
Bradley C C, Sacket C A, Tollet J J and Hulet R G 1997 *Phys. Rev. Lett.* **78** 985
[4] Davis K B, Mewes M-O, Anderson M R, van Druten N J, Kurn D M and Ketterle W 1995 *Phys. Rev. Lett.* **75** 3969
[5] Thorsheim H R, Weiner J, Julienne P S 1987 *Phys. Rev. Lett.* **58** 2420
[6] Miller J D, Cline R A and Heinzen D J 1994 *Phys. Rev. Lett.* **71** 2204
Cline R A, Miller J D and Heinzen D J 1994 *Phys. Rev. Lett.* **73** 632
[7] Ratliff L P, Wagshull M E, Lett P D, Rolston S L and Phillips W D 1994 *J. Chem. Phys.* **101** 2638
[8] McAlexander W I, Abraham E R I, Ritchie N W M, Williams C J, Stoof H T C and Hulet R G 1995 *Phys. Rev.* A **51** 871
[9] Napolitano R, Weiner J, Williams C J and Julienne P S 1994 *Phys. Rev. Lett.* **73** 1352
[10] Gardner J R, Cline R A, Miller J D, Heinzen D J, Boesten H M J M and Verhaar B J 1995 *Phys. Rev. Lett.* **74** 3764
[11] Weiner J, Bagnato V S, Zilio S and Julienne P S 1997 unpublished
[12] Lett P D, Julienne P S and Phillips W D 1995 *Ann. Rev. Phys. Chem.* **46** 423
Abraham E R I, McAlexander W I, Stoof H T C and Hulet R G 1996 *Phys. Rev.* A **53** 3092
Williams C J and Julienne P S 1994 *J. Chem. Phys.* **101** 2634
[13] Movre M and Pichler G 1977 *J. Phys. B: At. Mol. Phys.* **10** 2631
[14] Boesten H M J M, Tsai C C, Verhaar B J and Heinzen D J 1996 *Phys. Rev. Lett.* **77** 5194
[15] Feshbach H 1992 *Theoretical Nuclear Physics, Part 1: Nuclear Reactions* (New York: Wiley)
[16] Boesten H M J M, Tsai C C, Gardner J R, Heinzen D J and Verhaar B J 1997 *Phys. Rev.* A **55** 636
[17] McAlexander W I, Abraham E R I and Hulet R G 1996 *Phys. Rev.* A **54** R5
McAlexander W I, Abraham E R I and Hulet R G 1995 *Phys. Rev.* A **51** R871
[18] McAlexander W I, Abraham E R I and Hulet R G 1996 *Phys. Rev.* A **54** R5
[19] Wang H, Li J, Gould P L and Stwalley W C 1997 *J. Chem. Phys.* **106** 7899
[20] Marinescu M, Dalgarno A, Tsai C C, Miller J D, Cline R A and Heinzen D J 1996 *Bull. Am. Phys. Soc.* **41** 1083
[21] Jones K M, Julienne P S, Lett P D, Phillips W D, Tiesinga E and Williams C J 1996 *Europhys. Lett.* **35** 85
[22] Verhaar B J, Gibble K and Chu S 1993 *Phys. Rev.* A **48** R3429
[23] Moerdijk A J, Stwalley W C, Hulet R G and Verhaar B J 1994 *Phys. Rev. Lett.* **72** 40
Moerdijk A J and Verhaar B J 1994 *Phys. Rev. Lett.* **73** 518
[24] Bussery B and Aubert-Frécon M 1985 *J. Chem. Phys.* **82** 3224

[25] Spiegelmann F, Pavolini D and Daudley J-P 1989 *J. Phys. B: At. Mol. Opt. Phys.* **22** 2465
[26] Volz U and Schmoranzer H 1996 *Phys. Scr.* T **65** 48
[27] Schlapp R 1937 *Phys. Rev.* **51** 342
Julienne P *et al* 1992 Private communication
[28] Mizushima M 1975 *The Theory of Rotating Diatomic Molecules* (New York: Wiley) p 233
[29] Mies F H, Williams C J, Julienne P S and Krauss M 1996 *J. Res. Natl. Inst. Stand. Technol.* **101** 521
[30] Abraham E R I, McAlexander W I, Sacket C A and Hulet R G 1995 *Phys. Rev. Lett.* **74** 1315
[31] Krauss M and Stevens W J 1990 *J. Chem. Phys.* **93** 4236
[32] Amiot C 1990 *J. Chem. Phys.* **93** 8591
[33] Taylor J R 1972 *Scattering Theory* (New York: Wiley)
[34] Cohen-Tannoudji C, Dupont-Roc J and Grynberg G 1992 *Atom–Photon Interactions* (New York: Wiley)